Acta Pharmaceutica Sinica B 2026;16(8):5200−5216

Chinese Pharmaceutical Association
Institute of Materia Medica, Chinese Academy of Medical Sciences

Acta Pharmaceutica Sinica B

www.elsevier.com/locate/apsb
www.sciencedirect.com

ORIGINAL ARTICLE

Cytoplasmic relocation of nuclear Ku70 by Bruceine A augments cGAS−STING pathway-mediated anti-tumor immunity

Kai Huang[a,†], Zhaohui Tang[a,†], Qin Gong[a,†], Jianing Peng[b], Yicheng Rong[a], Tiancong Wu[c], Weichen Song[a], Siyu Mao[a], Yugui Xia[d], Wenjie Guo[a,*], Wen Liu[a,*]

[a]*State Key Laboratory of Pharmaceutical Biotechnology, Department of Gastroenterology, Nanjing Drum Tower Hospital, School of Life Science, Nanjing University, Nanjing 210093, China*
[b]*Faculty of Life Sciences, University College London, Gower Street, London WC1E6BT, UK*
[c]*Department of Radiation Oncology, Nanjing Jinling Hospital, Affiliated Hospital of Medical School, Nanjing University, Nanjing 210002, China*
[d]*Institute of Artificial Intelligence Biomedicine, Nanjing University, Nanjing 210093, China*

Received 11 July 2025; received in revised form 7 November 2025; accepted 4 June 2026

KEY WORDS

Colorectal cancer;
Anti-tumor immunity;
Ku70;
DNA damage repair;
cGAS−STING signal;
Bruceine A;
Radiotherapy;
Chemotherapy

Abstract DNA-damaging agents combined with agonists of the cGAS−STING pathway can effectively suppress colorectal cancer (CRC) by inducing cancer cell death and eliciting an antitumor immune response. In this study, we demonstrate that the natural compound Bruceine A (BA) inhibits CRC progression through a dual mechanism involving nuclear-to-cytoplasmic translocation of Ku70. Cytoplasmic Ku70 loses its canonical DNA repair function while simultaneously enhancing its interaction with cGAS, leading to increased cGAS oligomerization and elevated levels of double-stranded DNA (dsDNA), both of which amplify cGAS−STING signaling. Furthermore, Bruceine A-mediated Ku70 translocation exacerbates DNA damage accumulation, further enhancing tumor immunogenicity. In the murine CRC model, Bruceine A significantly inhibited tumor growth and enhanced tumor sensitivity to chemotherapy, radiotherapy, and anti-PD-1 treatment. Notably, genetic ablation of STING and $CD8^+$ T cells in mice substantially abolished the antitumor effects of Bruceine A, confirming its reliance on cGAS−STING activation and adaptive immunity. Our findings establish Ku70 as a novel therapeutic target in CRC, where its

*Corresponding authors.
E-mail addresses: guowj@nju.edu.cn (Wenjie Guo), liuwen@nju.edu.cn (Wen Liu).
†These authors made equal contributions to this work.
Peer review under the responsibility of Chinese Pharmaceutical Association and Institute of Materia Medica, Chinese Academy of Medical Sciences.

https://doi.org/10.1016/j.apsb.2026.06.010

subcellular redistribution disrupts genomic stability and bridges innate immune activation, synergistically promoting tumor cell death and antitumor immunity. Modulating Ku70 localization thus represents a promising strategy to enhance CRC treatment.

1. Introduction

Colorectal cancer (CRC) ranks as the third-highest in incidence and the second-highest mortality rate among all cancers globally[1]. Recent epidemiological studies have revealed an alarming increase in CRC cases among individuals under 50 years old[2−4], and both the incidence and mortality rates have shown a steady upward trend[5]. Research predicts that approximately 2.5 million new cases of CRC will occur by 2035 globally, with a particularly concerning increase in developing countries[6]. For first-line treatment of advanced or metastatic CRC, clinicians typically employ a combination of chemotherapy agents, such as FOLFOX (5-fluorouracil and oxaliplatin), FOLFIRI (5-fluorouracil and irinotecan), CAPOX (XELOX, capecitabine, and oxaliplatin), as well as FOLFOXIRI (5-fluorouracil, oxaliplatin, and irinotecan)[7,8]. When first-line treatment fails or the disease progresses, second-line treatment options involving various combinations of chemotherapy, targeted therapy, and immunotherapy should be considered[9,10]. Despite these therapeutic options, given the limited success of existing therapies, the development of new and more effective treatment strategies for CRC remains an urgent priority.

The cytoplasmic innate immune signal activation by sensing double-stranded DNA (dsDNA) leads to potent immune responses, which significantly impact the progression and prognosis of inflammatory diseases and cancer[11−13]. Upon detecting cytosolic DNA, cyclic GMP−AMP synthase (cGAS) synthesizes the second messenger 2′,3′-cyclic GMP−AMP (cGAMP), which subsequently binds to STING to trigger type I interferon signaling, ultimately enhancing anti-tumor immune responses[14−17]. Previous investigations have demonstrated that cGAS remains inactive within the nucleus due to its interaction with the acidic pockets formed by histones H2A and H2B[18−20]. Furthermore, nucleosome disruption resulting from DNA damage causes the release of cGAS from the nucleus into the cytoplasm to sense dsDNA[21,22]. Consequently, the sensing of dsDNA and subsequent STING activation is exclusively mediated by cytoplasmic cGAS, while intranuclear cGAS remains functionally distinct. In addition, the cGAS-Ku80 complex amplifies the interaction between DNA-PKcs and USP7, thereby boosting the stability of DNA-PKcs proteins and classical non-homologous end joining (NHEJ)[23]. Therefore, intranuclear cGAS (inactive cGAS) increases DNA damage repair to inhibit dsDNA release.

Ku70 is a protein encoded by the *XRCC6* gene. It plays a crucial role in DNA damage repair by binding to double-stranded DNA breaks in the nucleus to form DNA-PK (DNA damage repair kinase) complexes with Ku80 and DNA-PKcs[24,25]. Recent studies have revealed that Ku70 overexpression enhances the host cell responses to HTLV-1 (Human T lymphotropic virus type 1) infection, where Ku70 senses ssDNA90 and increases IFN-β production through STING[26]. Furthermore, DNA−PK forms complexes with Ku70 and Ku80 to trigger IRF3-mediated type I interferon responses in cGAS-deficient cancer cells upon dsDNA stimulation[27]. In addition to its nuclear functions, cytoplasmic Ku70 has been shown to trigger type III interferon production in response to bacterial and viral DNA[28−30]. Ku70 is recruited to *Rickettsia conorii* entry sites at the plasma membrane, thereby facilitating *Rickettsia conorii* internalization into nonphagocytic mammalian cells[31]. Recent studies have demonstrated that Ku70 is involved in recognizing accumulated cytoplasmic DNA in aging $CD4^+$ T cells to drive $CD4^+$ T cell activation, indicating Ku70's importance in senescence-associated autoimmunity[32]. While both Cytoplasmic and nuclear Ku70 participate in interferon signal activation, how the translocation of nuclear Ku70 to the cytoplasm affects cGAS−STING and interferon signals remains unclear.

In this study, we discovered that Bruceine A, a small-molecule compound, enhanced the interaction between Ku70 and cGAS; meanwhile, both proteins translocate from the nucleus to the cytoplasm, thereby activating the cGAS−STING and interferon signaling pathways to enhance anti-tumor immunity. Our findings highlight the dual functions of cGAS in DNA damage repair and dsDNA sensing and demonstrate that Ku70 mediates the translocation of cGAS from the nucleus (inactive state) to the cytoplasm (active state), thus facilitating dsDNA sensing and STING activation. Furthermore, the decrease of nuclear cGAS and Ku70 simultaneously enhances DNA damage to release dsDNA sensed for recognition by cGAS. Therefore, our elucidation of the Ku70-mediated cGAS−STING interferon activation pathway provides a novel therapeutic strategy for CRC treatment.

2. Materials and methods

2.1. Cell culture

The human colon cancer cell line (HCT-116), human embryonic kidney cell line (HEK293T), and human acute monocytic leukemia cells (THP-1) were purchased from the Shanghai Cell Bank of the Chinese Academy of Sciences (Shanghai, China). The mouse colon cancer cell line (MC-38) was purchased from KeyGEN BioTECH (Nanjing, China). These cells were cultivated in McCoy's 5A (01-075-1ACS, Biological Industries, Kibbutz Beit Haemek, Israel), PRMI 1640 (11,875,085, Gibco, Grand Island, NY, USA), and DMEM high-glucose (01-056-1A, Biological Industries) supplemented with 10% FBS (C04001-500, Biological Industries) and cultured in a humidified incubator with 5% CO_2 at 37 °C. All cell lines tested negative for mycoplasma contamination.

2.2. Mice

All C57BL/6J and BALB/c nude mice were purchased from Charles River (Beijing, China). All mice were housed in a specific pathogen-free facility at the Laboratory Animal Center, School of Life Science, Nanjing University. They were maintained with free

access to pellet food and water in plastic cages at 21 ± 2 °C and kept on a 12 h light/dark cycle. Mice were assigned to experimental groups using simple randomization. Animal welfare and experimental procedures were carried out by the Guide for the Care and Use of Laboratory Animals (Ministry of Science and Technology of China, 2006) and the related ethical regulations of Nanjing University (Approved number: IACUC-2407002-1). All efforts were made to minimize animals' suffering and to reduce the number of animals used. All studies involving animals are reported following the ARRIVE guidelines for reporting experiments involving animals.

2.3. Antibodies, plasmids, and reagents

Anti-γH2AX (Cat. number: ab26350, RRID: AB_297813) antibody, anti-CD8 (Cat. number: ab217344, RRID: AB_2890649), and anti-Histone H3 (Cat#ab219407) were from Abcam (Waltham, MA, USA). Anti-TBK1 (Cat. number: 67211-1-Ig, RRID: AB_3076688), anti-IRF3 (Cat. number: 11312-1-AP, RRID: AB_2127004), anti-*p*-IRF3 (Ser396) (Cat. number: 29528-1-AP, RRID: AB_2935415), anti-cGAS (Cat#26416-1-AP, RRID: AB_2880507), anti-Ku70 (Cat#66607-1-Ig, RRID: AB_2881967), anti-Ku80 (Cat. number: 16389-1-AP, RRID: AB_2257509), anti-DNA-PKcs (Cat. number: 28534-1-AP, RRID: AB_2881165), anti-Parp1 (Cat. number: 13371-1-AP, RRID: AB_2160459), and anti-STING (Cat. number: 19851-1-AP, RRID: AB_10665370) antibodies were from Proteintech (Wuhan, China). Anti-*p*-TBK1 (Ser172) (Cat. number: P00261) was from Boster (Wuhan, China). Anti-PCNA (Cat. number: sc-25280, RRID: AB_628109) and anti-dsDNA (Cat. number: sc-80772, RRID: AB_2745751) antibodies were from Santa Cruz (Dallas, CA, USA). Anti-β-tubulin (Cat. number: M20005S, RRID: AB_2920648) and anti-GAPDH (Cat. number: M20006, RRID: AB_2737054) antibodies were from Abmart (Shanghai, China). Anti-IFN-β (Cat. number: YT5964) antibody was from Immunoway (Plano, TX, USA). Anti-IFN-γ (Cat. number: 105,995) was from SinoBiological (Beijing, China). Anti-*p*-cGAS (S420) (Cat. number: AP1228) was from Abclonal (Wuhan, China). Anti-p-STING (Ser365) (Cat. number: 72,971, RRID: AB_2799831) was from Cell Signaling (Beverly, MA, USA).

The mouse pLV3-sh*Xrcc6*, mouse pLV3-sh*Sting1*, and human pLV3-sh*XRCC6* plasmids were from General Biol Co., Ltd (Chuzhou, China). The pimEJ5GFP, pCBASceI, pMD2, pRSV-Rev, and pMDLg/pRRE plasmids were from Addgene (Cambridge, MA, USA). pTac-GST-XRCC6 (human)-3 × HA, pT7-6 × His-SUMO-CGAS (human-opt-ecloi), pCMV-3 × Flag-EGFP-*XRCC6*, pCMV-3 × Flag-EGFP- *XRCC6*-R363A-R403A, and pCMV-mCherry-cGAS-3 × HA were from MiaoLingBio (Wuhan, China).

Oxaliplatin (Cat. Number: T0164), C-716 (Cat. number: T5154), SR-717 (Cat. number: T8655), and Bruceine A (Cat. Number: T2S2046) were from TargetMol (Boston, MA, USA). TRIZOL (Cat. number: 9109) was from Kakara (Dalian, China). PMA (Cat. number: P8139-5 MG) and NaF (Cat. number: S7920) were from Sigma−Aldrich (St. Louis, MO, USA). PMSF (Cat. number: ST505) was from Beyotime (Shanghai, China). DAPI (Cat. number: S2110) was from Solarbio (Beijing, China). Protein A/G beads (Cat. number: SA032025) were from Smart-Lifesciences (Changzhou, China). Hieff Trans Liposomal Transfection Reagent (Cat. number: 40802ES02) was from Yeasen Biotechnology (Shanghai, China). Quant-iT PicoGreen dsDNA Assay Kit (Cat. number: P7589) was from Thermo Fisher Scientific (Waltham, MA, USA). The HiScript III RT SuperMix (+gDNA wiper) (Cat. number: R323) and the Taq Pro Universal SYBR qPCR Master Mix (Cat. number: Q712-02) were from Vazyme (Nanjing, China).

2.4. RNA-sequencing analysis

HCT-116 cells were treated with 0.3 μmol/L Bruceine A. Total RNA was extracted using TRIZOL reagent, and RNA purity was quantified using a NanoDrop 2000 spectrophotometer (Thermo Fisher Scientific). RNA integrity was evaluated using an Agilent 2100 Bioanalyzer (Agilent Technologies, Santa Clara, CA, USA). RNA libraries were prepared according to the manufacturer's instructions using the NEBNext Ultra II Directional RNA Library Prep Kit for Illumina. The isolated RNA molecules were reverse transcribed to cDNA, amplified to primed cDNA molecules, and sequenced using an Illumina Novaseq 6000 with 150-base paired-end reads. All reads were aligned to the reference genome using Hisat2 v2.0.5 with default settings. Volcano plots, heatmap plots, KEGG, and GO analyses were performed using the Data Analysis Cloud Platform from Novogene Co., Ltd. (Beijing, China).

2.5. Subcutaneous tumor model

The C57BL/6J and BALB/c nude mice were subcutaneously implanted with 1×10^6 MC-38 cells. All mice received Bruceine A, oxaliplatin, C-176, anti-PD-1, and irradiation. Details are as follows: Bruceine A, 1, 2, 4 mg/kg, intraperitoneal, once a day; oxaliplatin, 2 mg/kg, intraperitoneal, twice a week; C-176, 14.4 mg/kg, intraperitoneal, once a day; anti-PD-1, 2 mg/kg, intraperitoneal, thrice a week; irradiation, 3 Gy, once. Solid tumors were harvested on Day 10, 12, or 14 from mice, weighed, and photographed.

2.6. Western blotting

HCT-116, MC-38, and THP-1 cells were treated with Bruceine A and C-176. After treatment, the cells were lysed using RIPA buffer (P0013B, Beyotime) supplemented with protease inhibitor PMSF on ice for 30 min. Insoluble components were removed through centrifugation at 12,000 rpm for 10 min, and the resulting lysates were then denatured by boiling in a loading buffer. The prepared samples were separated using SDS-polyacrylamide gel electrophoresis (SDS−PAGE) and transferred onto PVDF membranes. Following blocking with 5% non-fat milk at room temperature for 2 h. The membranes were incubated with primary antibody at 4 °C overnight, followed by washing 3 times in 1 × TBS-T and then incubated with secondary mouse antibody (RGAM001, Proteintech) and rabbit antibody (SA00001-2, Proteintech) for 2 h at room temperature. Detection was carried out using the chemiluminescence instrument (BIO-RAD, Hercules, CA, USA).

2.7. Lentiviral production and gene knockdown

HEK293T cells were transfected with pMD2.G, pRSV-Rev, pMDLg/pRRE, mouse pLV3-sh*Xrcc6*, human pLV3-sh*XRCC6*, and mouse pLV3-sh*Sting1*. Medium was replaced 16 h after transfection and was collected 48 h later, filtered at 0.45 μm to get the lentiviral liquid. Following this, lentiviral fluids were applied to infect MC-38 or HCT-116 cells for 48 h to disrupt the expression of Ku70 and STING. The short hairpin RNA sequences are as follows:

Mouse-sh*Xrcc6*: GGATCTTCCTTGACTTGATGC;
Human-sh*XRCC6*: CGACATAAGTCGAGGGACTTT;
Mouse-sh*Sting1*: AGAGGTCACCGCTCCAAATAT.

2.8. Tissue immunofluorescence and immunohistochemical

Tumor tissue sections were dewaxed, and antigen retrieval was performed using sodium citrate[33]. Sections were permeabilized with 0.2% Triton X-100 for 20 min and blocked with 5% BSA in PBS. Tissues were incubated overnight at 4 °C with primary antibodies against Ku70, STING, cGAS, γH2AX, dsDNA, and CD8. The following day, sections were washed three times with PBS-T and incubated for 2 h with Alexa Fluor 594-conjugated goat anti-mouse IgG (H + L) and Alexa Fluor 488-conjugated goat anti-rabbit IgG (H + L) secondary antibodies (Thermo Fisher Scientific) in the dark. Nuclei were counterstained with DAPI. Tissue samples were imaged using a TCS SP8 confocal microscope (Leica, Wetzlar, Germany). For immunohistochemistry, tissues were incubated overnight at 4 °C with primary antibodies, then stained using an Anti-mouse/rabbit Universal Immunohistochemical Detection Kit (PK10006, Proteintech). Results were captured using an Olympus microscope (Tokyo, Japan).

2.9. Cellular immunofluorescence

Cells were fixed with 4% formaldehyde for 20 min and permeabilized with 0.2% Triton X-100 for 20 min. Nonspecific binding was blocked with 5% BSA in PBS for 1 h at room temperature. Cells were incubated with primary antibodies (anti-STING, anti-cGAS, anti-Ku70, anti-dsDNA, and anti-γH2AX) overnight at 4 °C. Following primary antibody incubation, cells were incubated with fluorescent secondary antibodies for 1.5 h in the dark. Images were captured using a TCS SP8 confocal microscope (Leica, Wetzlar, Germany).

2.10. DNA damage repair examination

HCT-116 and HEK293T cells were cultured in 6-well plates and co-transfected with pCBASceI (1.5 μg) and pimEJ5GFP (1 μg) plasmids using Hieff Trans Liposomal Transfection Reagent. Following transfection, cells were treated with Bruceine A for 24 h. Cells were then suspended in PBS and analyzed for GFP-positive cells using a flow cytometer (Thermo Fisher Scientific, Waltham, MA, USA). Data analysis was performed using FlowJo 10.0 software.

2.11. Co-immunoprecipitation

HCT-116 cells were treated with Bruceine A and lysed in lysis buffer (P0013, Beyotime). Lysates were centrifuged at 12,000×*g* for 10 min to remove debris. Supernatants were incubated with anti-Ku70 or anti-cGAS antibodies overnight at 4 °C, followed by incubation with Protein A/G beads (SA032025, Smart-Lifesciences) for an additional night at 4 °C. Immunoprecipitates were washed eight times with 1 × PBS, boiled, and analyzed by Western blotting.

2.12. Real-time quantitative PCR (RT-qPCR)

HCT-116, MC-38, and THP-1 cells were cultured in 12-well plates. Total RNA was extracted using TRIZOL reagent (9109, Takara, Kyoto, Japan), and RNA concentration was measured using a Nanodrop instrument (Thermo Fisher Scientific, Waltham, MA, USA). RNA was reverse-transcribed into cDNA at 37 °C for 15 min, followed by 5 s at 85 °C, using HiScript III RT SuperMix for RT-PCR (+gDNA wiper). Real-time quantitative PCR was performed using Taq Pro Universal SYBR qPCR Master Mix. The primers of genes were as follows:

Human *IFNB1*: Forward Sequence (5′−3′): ACGCCGCATT GACCATCTAT; Reverse Sequence (5′−3′): GTCTCATTCCAGC CAGTGCT;

Human *CCL5*: Forward Sequence (5′−3′): CTGCTTTGCCT ACATTGCCC; Reverse Sequence (5′−3′): TCGGGTGACAAA GACGACTGC;

Human *CXCL10*: Forward Sequence (5′−3′): AGCAGAGGA ACCTCCAGTCTH; Reverse Sequence (5′−3′): AGGTACTCCTT GAATGCCACT;

Human *ACTB*: Forward Sequence (5′−3′): CGCGAGAGAA GATGACCCAGATC; Reverse Sequence (5′−3′): GCCAGAGGC GTACAGGGATA;

Mouse *Ifnb1:* Forward Sequence (5′−3′): CAGCTCCAAG AAAGGACGAACC; Reverse Sequence (5′−3′): GGCAGTGTA ACTCTTCTGCAT;

Mouse *Ccl5*: Forward Sequence (5′−3′): TTTGCCTACCTC TCCCTCGA; Reverse Sequence (5′−3′): CGACTGCAAGATTG GAGCACT;

Mouse *Cxcl10*: Forward Sequence (5′−3′): CCAAGTGCTG CCGTCATTTTC; Reverse Sequence (5′−3′): GGCTCGCAGGG ATGATTTCAAC;

Mouse *Actb*: Forward Sequence (5′−3′): GGCTGTATTCC CCTCCATCG; Reverse Sequence (5′−3′): CCAGTTGGTAACA ATGCCATGT.

2.13. Nucleocytoplasmic separation

HCT-116 cells were treated with Bruceine A, resuspended in Lysis Buffer (10 mmol/L HEPES, 1.5 mmol/L $MgCl_2$, 10 mmol/L KCl, 0.5 mmol/L DTT, 1 mmol/L PMSF), and lysed on ice for 30 min. NP40 was added to a final concentration of 2%, and cells were incubated on ice for 1 h. Cells were centrifuged at 12,000×*g* at 4 °C. The supernatant was collected as the cytoplasmic fraction. The procedure was repeated twice, discarding the last two cytoplasmic fractions. The pellet was lysed with RIPA buffer and designated as the nuclear fraction. Loading buffer was added to both fractions, and samples were heated at 100 °C for 10 min.

2.14. Limited proteolysis-small molecule mapping (Lip-SMap) assay

Lip-Map assay was performed as reported previously[34]. The total proteome of HCT-116 cells was divided into two groups, each with a protein concentration of at least 2 μg/μL. One group was treated with Bruceine A (0.3 μmol/L) for 10 min at room temperature, while the other was treated with DMSO. Both groups were then treated with Proteinase K at a 1:100 proteinase K to substrate mass ratio for 5 min at room temperature. Samples were heated at 98 °C for 3 min in a thermal cycler. Sodium deoxycholate was added to a final concentration of 5% to stop the digestion reaction, followed by further heating at 98 °C for 3 min. Complete digestion was carried out under denaturing conditions. Protein fragments were reduced with 5 mmol/L TCEP for 40 min at 37 °C, then alkylated with 20 mmol/L iodoacetamide for 30 min at 25 °C in the dark. Samples were diluted with 0.1 mol/L ammonium bicarbonate to a final concentration of 1% sodium deoxycholate. All samples underwent mass spectrometry analysis by ChomiX Biotech Co., Ltd (Nanjing, China).

2.15. dsDNA level detection

The Quant-iT PicoGreen dsDNA Assay Kit (P7589, Thermo Fisher Scientific) was used to analyze dsDNA levels in cell supernatants from HCT-116 and THP-1 cells[35]. Samples were excited at 485 nm, and fluorescence intensity was measured at 520 nm using a Multi-Functional Microplate Detector (TECAN, Männedorf, Switzerland).

2.16. Cellular thermal shift assay (CESTA)

HCT-116 cells were incubated with DMSO or Bruceine A for 3 h, collected, and subjected to a CETSA[36]. Briefly, HCT-116 cells were equally divided into 10 parts, and the cells were heated for 3 min at various temperatures (43, 46, 49, 52, 55, 58, 61, 64, 67, and 70 °C). The heated cells were kept at liquid nitrogen for 1 min, transferred to room temperature for 3 min, and this sequence was repeated three times. Cell lysates were extracted by centrifugation at 12,000×*g* for 10 min. The Ku70, Ku80, and DNA-PKcs protein levels were detected using Western blotting.

2.17. Blood routine examination

C57BL/6J mice received Bruceine A (4 mg/kg, i.p., once a day) from Day 0 to Day 14. Fresh blood (50 μL) was isolated from C57BL/6J mice on Day 14. The number of White blood cells, neutrophils, Hemoglobin, lymphocytes, red blood cells, and platelets in blood was detected using a Fully Automatic Blood Cell Analyzer (BC-5000 Vet, Mindray, Shenzhen, China).

2.18. Analysis of liver and kidney function

Fresh blood was centrifuged at 3000×*g* for 10 min to get serum. The AST (Aspartate aminotransferase), ALT (Alanine aminotransferase), UA (Uric acid), and CRT (Creatinine) levels in serum were detected using the Aspartate aminotransferase Assay Kit (C010-2-1, Nanjing Jiancheng Bioengineering Institute), Alanine aminotransferase Assay Kit (C009-2-1, Nanjing Jiancheng Bioengineering Institute), Uric acid Test Kit (C012-2-1, Nanjing Jiancheng Bioengineering Institute), and Creatinine Assay kit (C011-2-1, Nanjing Jiancheng Bioengineering Institute).

2.19. Protein expression and purification

The expression and purification of human Ku70 (hKu70) and human cGAS (hcGAS) were performed as described in previous reports[37,38]. pTac-GST-XRCC6 (human)-3 × HA or pT7-6 × His-SUMO-cGAS (human-opt-ecloi) plasmids were transformed into *E. coli* BL21 DE3 cells and cultured in LB medium at 37 °C in an incubator. When the bacterial OD (600 nm) reached 0.6−0.8, 0.5 μmol/L IPTG (ST098, Beyotime) was added, and the cells were cultured at 18 °C for 18 h. The cells were harvested and resuspended in lysis buffer containing 25 mmol/L Tris-HCl, pH 8.0, 300 mmol/L NaCl, and 0.5 mmol/L PMSF. GST-HA-Ku70 protein was captured using a GST affinity column (P2262, Beyotime) and eluted with 10 mmol/L Glutathione (Y270851, Beyotime) in a buffer containing 250 mmol/L Tris and 150 mmol/L NaCl. His-SUMO-cGAS protein was purified by affinity chromatography using a Ni-NTA column (Qiagen, Düsseldorf, Germany). The protein was further purified by gel filtration (Superdex 200 10/300 GL column, GE Healthcare, Marlborough, MA, USA).

2.20. Microscale thermophoresis (MST)

For Bruceine A bound to EGFP-Ku70 (WT and R363A-R403A) from HEK293T cell lysates. The diluted EGFP-Ku70 and Bruceine A were mixed with an equal volume. For the purified cGAS−Ku70 MST assay, buffer exchange and fluorescent dye labeling were performed on 10 μmol/L human GST-HA-Ku70 according to the Monolith NT RED-NHS Next-Generation Protein Labeling Kit. The diluted human His-SUMO-cGAS and human GST-HA-Ku70 were mixed with an equal volume. MST assays were subsequently performed using a Monolith NT.115 (NanoTemper, Munich, Germany). MO.Affinity analysis software was used for the combined analysis.

2.21. Pull-down assay

For cGAS−Ku70 pull-down, human His-SUMO-cGAS (10 μg) and human GST-HA-Ku70 (10 μg) were mixed in 400 μL pull-down buffer overnight at 4 °C. The GST beads (Smart-Lifesciences) and Ni-NTA beads (Smart-Lifesciences) were incubated with the mixed proteins overnight at 4 °C. Excess proteins of hcGAS and hKu70 were washed off the beads using PBS 5 times, and 60 μL loading buffer was added and boiled for 15 min 30 μL supernatant was analyzed by SDS−PAGE. The protein bands were visualized by Coomassie blue staining.

2.22. Enzyme-linked immunosorbent assay (ELISA)

Supernatants from HCT-116 and THP-1 cells were centrifuged at 2000×*g* for 5 min to remove cell debris. The IFN-β levels in supernatants were detected using the Human IFN-β ELISA Kit (E-EL-H0085, Elabscience, Wuhan, China).

2.23. Quantification and statistical analysis

Data are expressed as mean ± standard error of the mean (SEM) of three independent experiments, and each experiment included triplicate sets. All data were statistically evaluated by one-way ANOVA, followed by Dunnett's test between the control and multiple-dose groups. In all cases, $^{**}P < 0.01$, $^{*}P < 0.05$, ns, not significant (ns, $P > 0.05$). All statistical analyses were performed using GraphPad (Prism 9) (RRID: SCR_002798).

3. Results

3.1. Bruceine A activates cGAS−STING and type I interferon signals

Firstly, we examined the effect of Bruceine A (BA), derived from the natural Chinese herb *Brucea brucei*, on interferon signaling by RNA-seq analysis. The results revealed that cGAS−STING activation-related genes were increased in the Bruceine A group compared with the control group (Fig. 1A and Supporting Information Fig. S1A and S1B). Bruceine A enhanced the mRNA levels of *IFNB1*, *CXCL10*, and *CCL5* in HCT-116 and PMA-primed THP-1 cells in a dose-dependent manner (Fig. 1B and D, Fig. S1C and S1D), and the protein expression levels of IFN-β in cellular supernatant showed the same result (Fig. 1C and E). TBK1 and IRF3 are two essential effectors downstream of the cGAS−STING pathway[39]. Western blotting analysis demonstrated that Bruceine A upregulated the phosphorylation of cGAS,

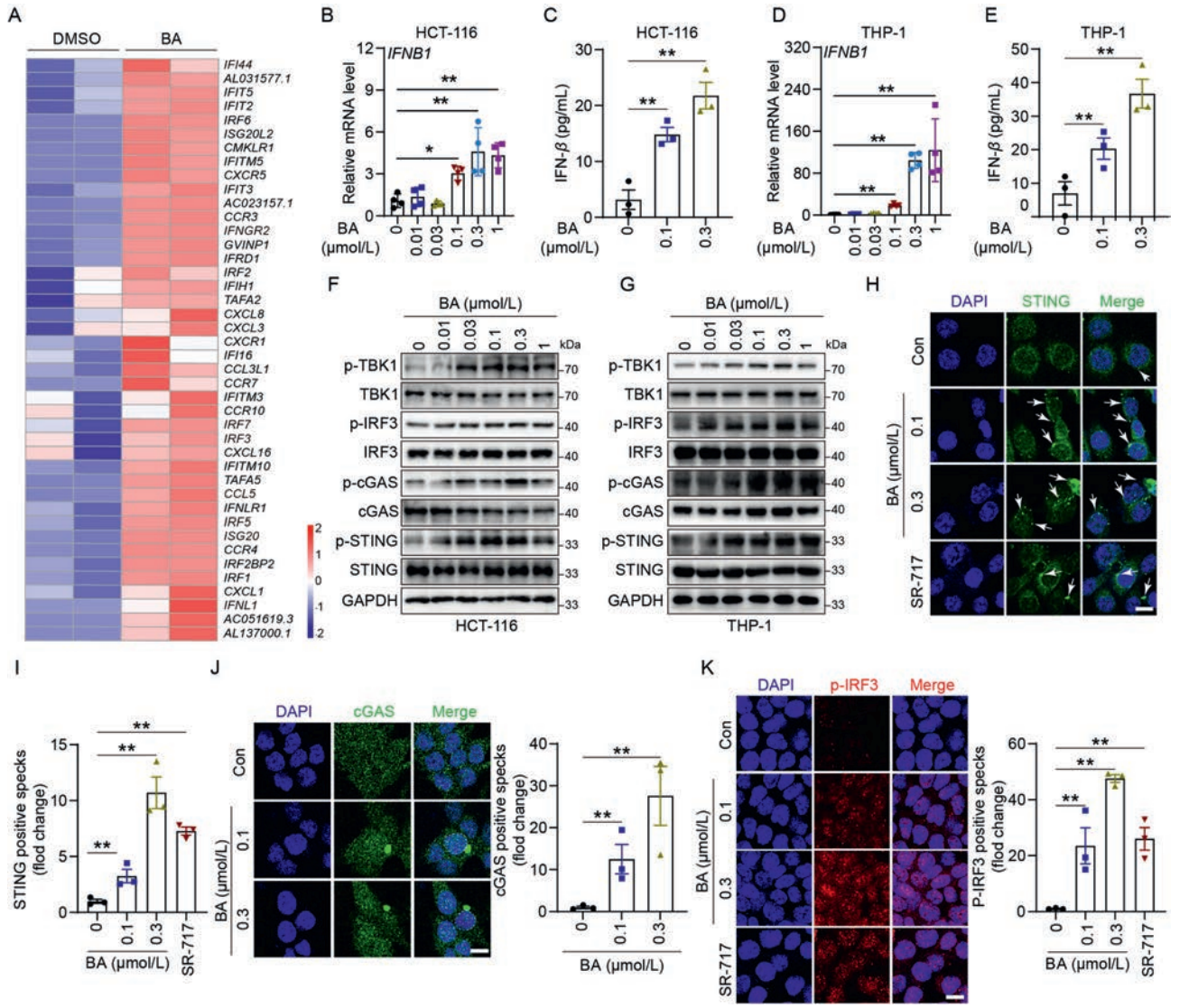

Figure 1 Bruceine A activates cGAS−STING and type I interferon signals (A) Heatmap of differentially expressed genes related to STING pathway activation from RNA-seq of HCT-116 cells treated with Bruceine A (BA, 0.3 μmol/L) for 12 h. Comparative expression of STING activation-associated genes is expressed as FPKM for each replicate (B, D) HCT-116 and PMA-primed THP-1 cells were treated with Bruceine A (0.01, 0.03, 0.1, 0.3, and 1 μmol/L) for 12 h, and the mRNA levels of *IFNB1* were detected by RT-qPCR (C, E) HCT-116 and PMA-primed THP-1 cells were treated with Bruceine A (0.1 and 0.3 μmol/L) for 12 h, and ELISA was used to analyze the IFN-β protein levels in the supernatant (F, G) Western blotting analysis of p-cGAS, cGAS, p-STING, STING, p-TBK1, TBK1, p-IRF3, and IRF3 in HCT-116 and PMA-primed THP-1 cells treated with Bruceine A (0.01, 0.03, 0.1, 0.3, and 1 μmol/L) for 6 h (H, I) Cellular immunofluorescence analysis of STING in HCT-116 cells treated with Bruceine A (0.1 and 0.3 μmol/L) and SR-717 (1 μmol/L), and quantitative analysis of STING specks. Scale bar: 75 μm (J) Cellular immunofluorescence analysis of cGAS in HCT-116 cells treated with Bruceine A (0.1 and 0.3 μmol/L). Quantitative analysis of cGAS speck is shown beside. Scale bar: 75 μm (K) Cellular immunofluorescence analysis of *p*-IRF3 in HCT-116 cells treated with Bruceine A (0.1 and 0.3 μmol/L) and SR-717 (1 μmol/L). Quantitative analysis of *p*-IRF3 is shown beside. Scale bar: 75 μm. The *P* values are indicated, $*P < 0.05$; $**P < 0.01$. Data are presented as mean ± SEM. Statistical analysis was performed using one-way ANOVA with Dunn's multiple-comparison test.

STING, TBK1, and IRF3 in tumor cells and macrophages (Fig. 1F and G). Immunofluorescence analysis showed that Bruceine A induced the number of cGAS and STING specks and the expression levels of p-IRF3 in tumor cells (Fig. 1H−K), suggesting Bruceine A activates cGAS and STING. These findings demonstrate that Bruceine A activates the cGAS−STING and type I interferon signals *in vitro*.

3.2. Bruceine A targets Ku70 to activate the cGAS−STING pathway

To explore the specific target proteins of Bruceine A, the LiP-SMap analysis was performed (Fig. 2A). The mass spectrometry analysis identified a decrease in two short Ku70 peptides and an increase in one long Ku70 peptide after cleavage by proteinase K

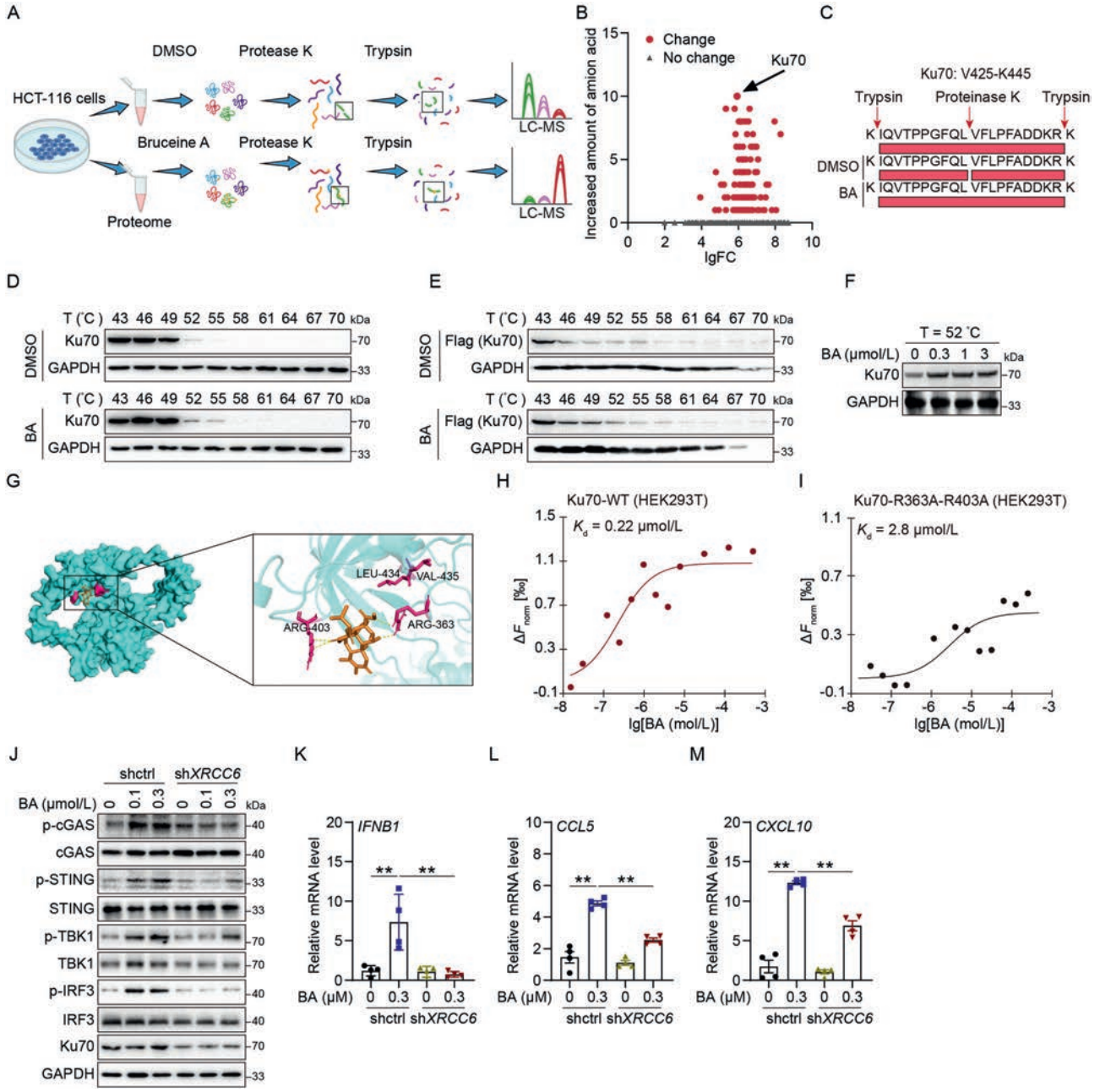

Figure 2 Bruceine A targets Ku70 to activate the cGAS−STING pathway (A) This diagram represents the systematic identification of protein-small molecule interactions using Lip-SMap (B) The scatter plot illustrates the targets of Bruceine A (3 μmol/L) filtered by Lip-SMap (C) Theoretical cleavage positions of Ku70 peptides (D) Cellular lysates from HCT-116 cells are treated with Bruceine A (3 μmol/L), and Western blotting analysis depicts the Cellular Thermal Shift Assay of the Ku70 protein (E) Cell lysates from HEK293T cells transfected with Flag-Ku70 plasmids were treated with Bruceine A (3 μmol/L) (F) Cellular lysates from HCT-116 cells were treated with Bruceine A (0.3, 1, and 3 μmol/L) at 52 °C (G) The Ku70 and Bruceine A binding model was predicted using molecular docking (H, I) EGFP-Ku70-WT and EGFP-Ku70-R363A-R403A plasmids were transfected into HEK293T cells, and the interaction of Ku70-WT and Ku70-R363A-R403A with Bruceine A was determined using MST (J) Western blotting analysis of p-cGAS, cGAS, p-STING, STING, p-TBK1, TBK1, p-IRF3, and IRF3 in shctrl and sh*XRCC6* (Ku70) HCT-116 cells treated with Bruceine A (0.1 and 0.3 μmol/L) for 6 h (K−M) HCT-116 cells were transfected with shctrl and sh*XRCC6* lentivirus, followed by Bruceine A (0.3 μmol/L) stimulation for 12 h. The *IFNB1*, *CCL5*, and *CXCL1*0 mRNA expression levels were measured using RT-qPCR. The *P* values are indicated, $^{**}P < 0.01$. Data are presented as mean ± SEM. Statistical analysis was performed using one-way ANOVA with Dunn's multiple-comparison test.

in Bruceine A-treated proteomes compared with the DMSO treatment (Fig. 2B and C). The interaction between Bruceine A and Ku70 was further reaffirmed through the cellular thermal shift assay (Fig. 2D−F), and based on the LiP−SMap results, a binding model of Ku70 to Bruceine A was predicted using Autodock and PyMol (Fig. 2G). Ku80 and DNA-PKcs participated in DNA damage repair[40], and cellular thermal shift assay results indicated that Bruceine A failed to interact with both of them (Supporting Information Fig. S2A). Bruceine A did not affect the expression levels of proteins associated with DNA damage repair, such as DNA-PKcs, Ku80, Ku70, and PARP1 in tumor cells (Fig. S2B). Further, the MST assay indicated that the dissociation constant of Bruceine A bound to Ku70 was 0.218 μmol/L, whereas according to the binding model, Ku70 mutants (Ku70-R363A-R403A) that interacted with Bruceine A had a bigger dissociation constant (2.815 μmol/L) compared with Ku70 WT (Fig. 2H and I). We next explored whether Ku70 affects the Bruceine A-induced cGAS−STING signal activation. Ku70 was silenced in colorectal cancer cells using lentivirus-mediated shRNA to test this hypothesis. Ku70 knockdown decreased *p*-cGAS, p-STING, *p*-TBK1, and *p*-IRF3 protein expression levels, as well as *IFNB1*, *CCL5*, and *CXCL1*0 mRNA levels induced by Bruceine A, indicating that the cGAS−STING-mediated type I interferon signal activated by Bruceine A depends on Ku70 (Fig. 2J−M). These results suggest that Bruceine A induces the cGAS−STING activation by targeting Ku70.

3.3. Bruceine A inhibited DNA damage repair by targeting Ku70

To investigate the molecular mechanism between Ku70 and cGAS−STING signal under Bruceine A stimulation, we established an experimental system to analyze whether Bruceine A affects DNA damage repair using flow cytometry. A site-specific double-strand break was generated by the I-SceI endonuclease[41], and the NHEJ-GFP reporter systems were utilized to evaluate the impact of Bruceine A on the NHEJ (Non-homologous end joining) pathway. Our results demonstrated that Bruceine A inhibited the NHEJ in a dose-dependent manner in HCT-116 and HEK293T cells (Fig. 3A−C). DNA damage leads to the release of double-stranded DNA (dsDNA) into both cytoplasmic and extracellular compartments. Western blotting and cellular immunofluorescence analysis revealed that Bruceine A significantly enhanced the γH2AX expression in cell lysates and the nucleus (Fig. 3D−F). Furthermore, Bruceine A increased the dsDNA levels in the cytoplasm and supernatant in HCT-116 cells and PMA-primed THP-1 cells (Fig. 3G−I). Additionally, we found that knockdown of Ku70 directly resulted in increased γH2AX expression in the cytoplasm as well as dsDNA levels in the cytoplasm and supernatant, and Bruceine A showed a minor promoting effect on γH2AX expression and dsDNA levels in sh*XRCC6* cells (Fig. 3J−M). Our findings showed that genetic ablation of Ku70 increases the γH2AX expression levels and dsDNA release in tumor cells, suggesting that Ku70 plays a crucial role in DNA damage repair, which is consistent with previous studies[42]. Interestingly, genetic ablation of Ku70-mediated DNA damage level did not appear to be significantly enhanced by Bruceine A, which suggests that Bruceine A activates cGAS−STING signaling by releasing dsDNA.

3.4. Bruceine A promoted cytoplasmic translocation of cGAS via Ku70

cGAS, a DNA sensor, is primarily expressed in the cellular nucleus and cytoplasm[43], but nuclear cGAS (inactive cGAS) cannot activate STING-mediated interferon activation[18,20,44]. The cGAS translocation from the nucleus to the cytoplasm represented a crucial mechanism for sensing dsDNA and activating the downstream signaling of cGAS[45,46]. Interestingly, cellular immunofluorescence analysis reveals that specks of cGAS localize at the nuclear membrane following Bruceine A treatment (Fig. 1J). Based on these observations, we hypothesize that Bruceine A induces translocation from the nucleus into the cytoplasm to sense dsDNA, potentially mediated by Ku70. Our results demonstrate that cGAS−Ku70 complexes are located in the nucleus, on the nuclear membrane, and in the cytoplasm after Bruceine A treatment, as revealed by cellular immunofluorescence (Fig. 4A). In contrast, knockdown of Ku70 inhibited Bruceine A-induced cGAS translocation from the nucleus, suggesting that Ku70 facilitates cGAS translocation into the cytoplasm from the nucleus (Fig. 4B). Next, we overexpressed EGFP-Ku70 and mCherry-cGAS in HEK293T cells. Fluorescent results showed that Bruceine A promoted the co-localization between Ku70 and cGAS near the nuclear membrane of the cell (Fig. 4C). Furthermore, we verified that Bruceine A enhances the interaction between Ku70 and cGAS in HCT-116 cells (Fig. 4D and E). Next, we expressed and purified the human His-SUMO-cGAS (1−522) and human GST-HA-Ku70 (1−609) recombinant proteins. Pull-down assay and MST assay showed that cGAS directly bound to Ku70 (K_d = 3.25 nmol/L) (Fig. 4F−H). Nucleocytoplasmic fractionation further confirms that Bruceine A promotes the nuclear export of cGAS (Fig. 4I and J). Our findings reveal the dual functions of Ku70 in DNA damage repair and the nuclear export of cGAS. The relocation of nuclear cGAS to the cytoplasm (inactive to active) was mediated by Ku70 to facilitate dsDNA sensing and STING activation. Notably, the decrease of nuclear Ku70 promotes DNA damage, leading to dsDNA release and subsequent sensing by cGAS (Fig. 4K). In conclusion, our findings elucidate a novel mechanism whereby Ku70 mediates cGAS translocation into the cytoplasm, enabling dsDNA sensing and subsequent activation of the cGAS−STING and interferon signaling.

3.5. Bruceine A inhibits tumor growth in vivo through a Ku70-dependent mechanism

Next, we verified the *in vivo* tumor growth inhibitory effect of Bruceine A by using a mouse subcutaneous tumor model (Supporting Information Fig. S3A). Bruceine dose-dependently inhibits tumor growth and activates the cGAS−STING pathway, in addition to eliciting a corresponding anti-tumor immune response (Fig. 5A−D and Fig. S3B−S3D). Interestingly, Bruceine A induced the colocalization between dsDNA and cGAS in tumor sections, suggesting again that Bruceine A activated the cGAS−STING signal *in vivo* (Fig. S3E). Subsequently, we established a murine model using Ku70-silenced MC-38 cells. We found that silencing Ku70 in tumor cells attenuates Bruceine A-induced tumor growth inhibition (Fig. 5E−G and Supporting Information Fig. S4A−S4C). Bruceine A increased the expression levels of *p*-TBK1, IFN-*β*, p-

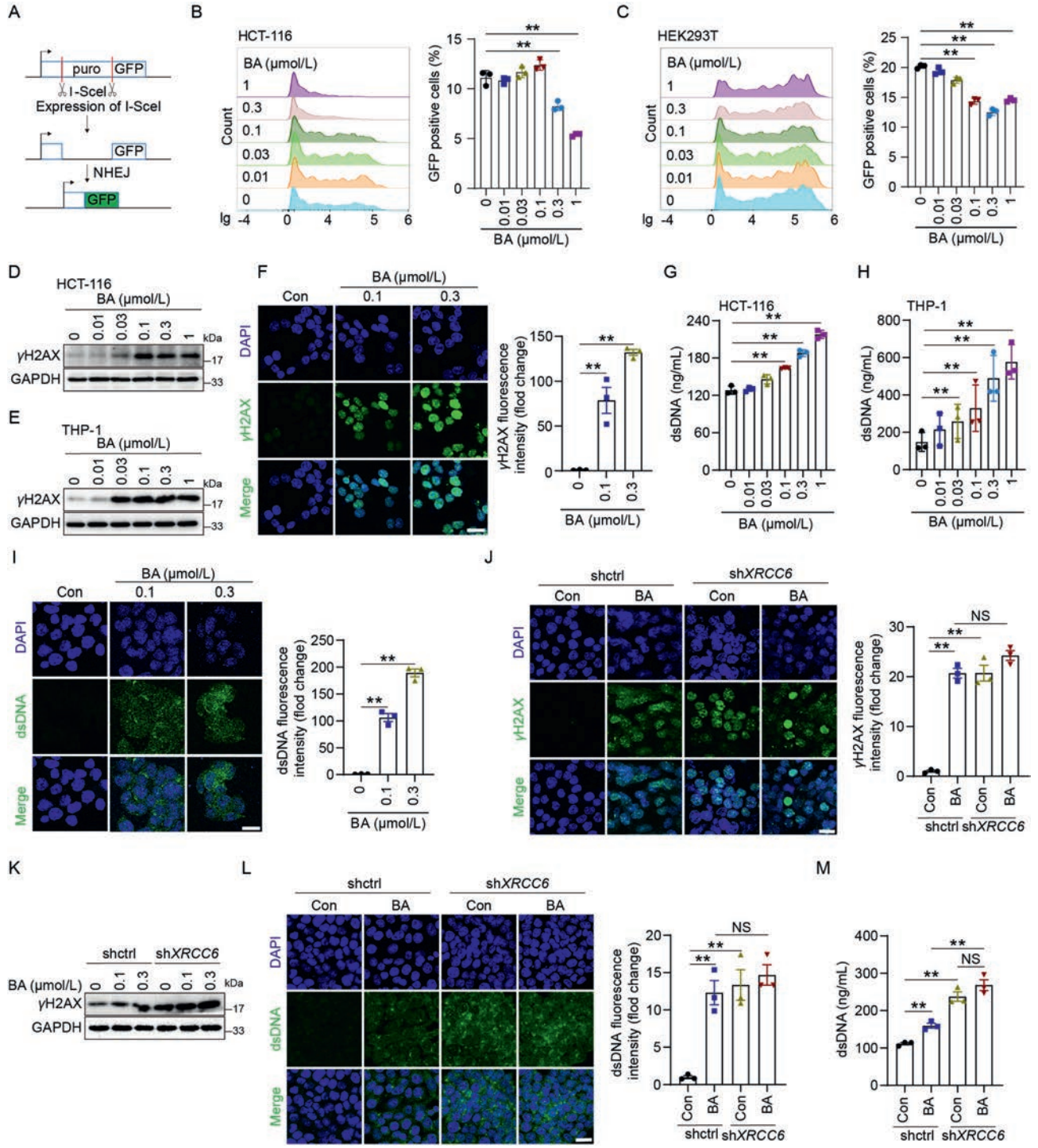

Figure 3 Bruceine A inhibits DNA damage repair *via* Ku70 (A−C) HCT-116 and HEK293T cells were seeded in 6-well plates and were co-transfected with pCBAScel and pimEJ5-GFP plasmids. Cells were incubated with Bruceine A for 24 h and analyzed using flow cytometry to detect the percent of GFP-positive cells (D, E) Western blotting analysis of γH2AX in HCT-116 and PMA-primed THP-1 cells treated with Bruceine A for 12 h (F) Immunofluorescence analysis for γH2AX in HCT-116 cells treated with Bruceine A (0.1 and 0.3 μmol/L) for 12 h. Quantitative analysis of γH2AX is shown beside. Scale bar: 75 μm (G, H) The dsDNA levels were detected in the supernatant from HCT-116 and THP-1 cells treated with Bruceine A for 12 h. The dsDNA levels in the supernatant were detected using Quant-iT PicoGreen dsDNA Assay Kit (I) Immunofluorescence analysis for dsDNA in HCT-116 cells treated with Bruceine A (0.1 and 0.3 μmol/L) for 12 h. Quantitative analysis of dsDNA is shown beside. Scale bar: 75 μm (J) Immunofluorescence analysis of γH2AX in shctrl and sh*XRCC6* HCT-116 cells treated with Bruceine A (0.1 and 0.3 μmol/L) for 12 h. Quantitative analysis of γH2AX is shown beside. Scale bar: 75 μm (K) Western blotting analysis for γH2AX in shctrl and sh*XRCC6* HCT-116 cells treated with Bruceine A (0.1 and 0.3 μmol/L) for 12 h (L) Immunofluorescence analysis of dsDNA in shctrl and sh*XRCC6* HCT-116 cells treated with Bruceine A (0.1 and 0.3 μmol/L) for 12 h. Quantitative analysis of dsDNA is shown beside. Scale bar:

STING, and IFN-γ and the number of $CD8^+$ T cells *in vivo*, and the knockdown of Ku70 limited Bruceine A's effect (Fig. 5H and Fig. S4C and S4D). Additionally, tissue immunofluorescence showed that Bruceine A dose-dependently induced an increase in the levels of γH2AX in the nucleus and dsDNA in tumor sections (Fig. 5I and J). These results suggest that Bruceine A inhibits colon cancer tumor growth *in vivo* by the exact mechanism of targeting Ku70.

3.6. Bruceine A-mediated tumor growth suppression requires STING activation

The preceding findings demonstrate that Bruceine A induces tumor growth suppression by activating the cGAS−STING signaling pathway. To further elucidate the relationship between Bruceine A and the cGAS−STING signal, we employed STING small-molecule inhibitor (C-176)[47], sh*Sting1* lentivirus, and *Sting1* knock-out mice. The RT-qPCR results demonstrated that C-176 significantly dampened the Bruceine A-induced the expression upregulation of *IFNB1* and *CXCL1*0 mRNA (Fig. 6A and B). Moreover, Western blotting analysis showed that C-176 inhibited Bruceine A-induced TBK1 and IRF3 phosphorylation (Fig. 6C). Consistently, the cGAS−STING pathway and interferon signaling activated by Bruceine A were reversed in MC-38 cells following genetic ablation of STING (Fig. 6D and E). In a murine model of CRC, administration of C-176 partially reversed tumor growth suppression caused by Bruceine A (Fig. 6F−H and Supporting Information Fig. S5A−S5C) and reduced the expression levels of p-TBK1, IFN-β, IFN-γ, and $CD8^+$ T cell infiltration (Fig. 6I and Fig. S5C and S5D). To validate these findings further, we investigated whether the antitumor effect of Bruceine A depended on STING in immune cells using *Sting1* knock-out mice. Our findings demonstrated that tumor growth suppression caused by Bruceine A was abolished in the *Sting1* knock-out mice (Fig. 6J−L and Fig. S5E−S5G). Furthermore, Bruceine A treatment failed to increase the expression levels of p-TBK1, IFN-β, and IFN-γ, and promote $CD8^+$ T cell infiltration in *Sting1* knock-out mice (Fig. 6M and Fig. S5G and S5H). These findings strongly suggest that Bruceine A-mediated tumor growth suppression is dependent on STING activation.

3.7. Inhibition of tumor growth caused by Bruceine A depends on the host's immune response

The cGAS−STING signal activation contributes to the antitumor response by inducing immune cell activation and infiltration[12,48,49]. To explore whether Bruceine A affects the immune response of various organs, we conducted a toxicity assessment experiment. Results indicated that Bruceine A did not affect the phenotype of the heart, liver, spleen, lung, and kidney (Supporting Information Fig. S6A), did not change the pathological morphology of liver and kidney (Fig. S6B), and did not alter the number of white blood cells, neutrophils, hemoglobin, lymphocytes, red blood cells, and platelets in peripheral blood (Fig. S6C−S6H). Bruceine A also did not affect liver and kidney function (Fig. S6I−S6L). Those results suggest that Bruceine A has no host toxicity *in vivo*.

To investigate the role of T cells in Bruceine A-mediated antitumor immunity, we utilized immunodeficient mice. Bruceine A failed to inhibit tumor growth in BALB/c nude mice (Fig. 7A−C and Supporting Information Fig. S7A and S7B). Notably, immunohistochemistry analysis showed that Bruceine A increases *p*-TBK1 and IFN-β levels in nude mice tumors (Fig. 7D). We further investigated the significance of $CD8^+$ T cells for Bruceine A-mediated anti-tumor immunity (Fig. S7C). Bruceine A exhibited negligible tumor suppression effects in CD8 knockout mice, which was consistent with the phenomenon observed in nude mice (Fig. 7E−G and Fig. S7D). Similarly, the expression levels of p-TBK1, IFN-β, and IFN-γ in CD8 knockout mice did not increase following the Bruceine A treatment compared to the wild-type mice (Fig. 7H and Fig. S7E). Collectively, these results demonstrate that Bruceine A-induced tumor growth inhibition requires the $CD8^+$ T cells.

3.8. Bruceine A sensitizes radiotherapy, chemotherapy, and immunotherapy

Colorectal cancer treatment heavily relies on radiotherapy, chemotherapy, and immunotherapy. A combination of various therapeutic approaches is often employed to treat patients with CRC[50−52]. Our experimental results demonstrate that Bruceine A enhances oxaliplatin and irradiation-induced tumor growth suppression in a murine model of CRC (Fig. 8A−C and E−G and Supporting Information Fig. S8). Mechanistically, Bruceine A upregulates oxaliplatin and irradiation-induced p-TBK1, IFN-β, and IFN-γ expression levels in tumor sections(Fig. 8D and H, Fig. S8C and S8F). To investigate whether Bruceine A impacts the tumor microenvironment (TME), flow cytometry was employed to detect T cell activation in tumor tissues. Our results showed that Bruceine A combined with oxaliplatin, increased the number percentage of Granzyme $B^+CD8^+CD45^+$ T cells and INF-$\gamma^+CD8^+CD45^+$ T cells (Supporting Information Fig. S9A−S9D) and decreased the number percentage of $FOXP3^+CD25^+CD4^+CD45^+$ T cells (Fig. S9E and S9F), suggesting that Bruceine A enhanced the immune response in the tumor microenvironment.

In the context of immunotherapy, Bruceine A significantly suppressed tumor growth in combination with anti-PD-1 antibody and enhanced the p-TBK1, IFN-β, and IFN-γ expression levels (Fig. 8I−L and Supporting Information Fig. S10A−S10C). Notably, the number of $CD8^+$ T cells was significantly elevated in the combination group compared with the anti-PD-1 monotherapy (Fig. S10D). Collectively, these findings suggest that the cGAS−STING signal activation induced by Bruceine A sensitizes radiotherapy, chemotherapy, and immunotherapy, providing a practical approach to treat colorectal cancer.

4. Discussion

Colorectal cancer (CRC) remains one of the most prevalent and lethal cancers globally, with increasing rates of incidence,

75 μm (M) The dsDNA levels in the supernatant from shctrl and sh*XRCC6* HCT-116 cells treated with Bruceine A (0.1 and 0.3 μmol/L) for 12 h. The *P* values are indicated, $^{**}P < 0.01$; NS, not significant. Data are presented as mean ± SEM. Statistical analysis was performed using one-way ANOVA with Dunn's multiple-comparison test.

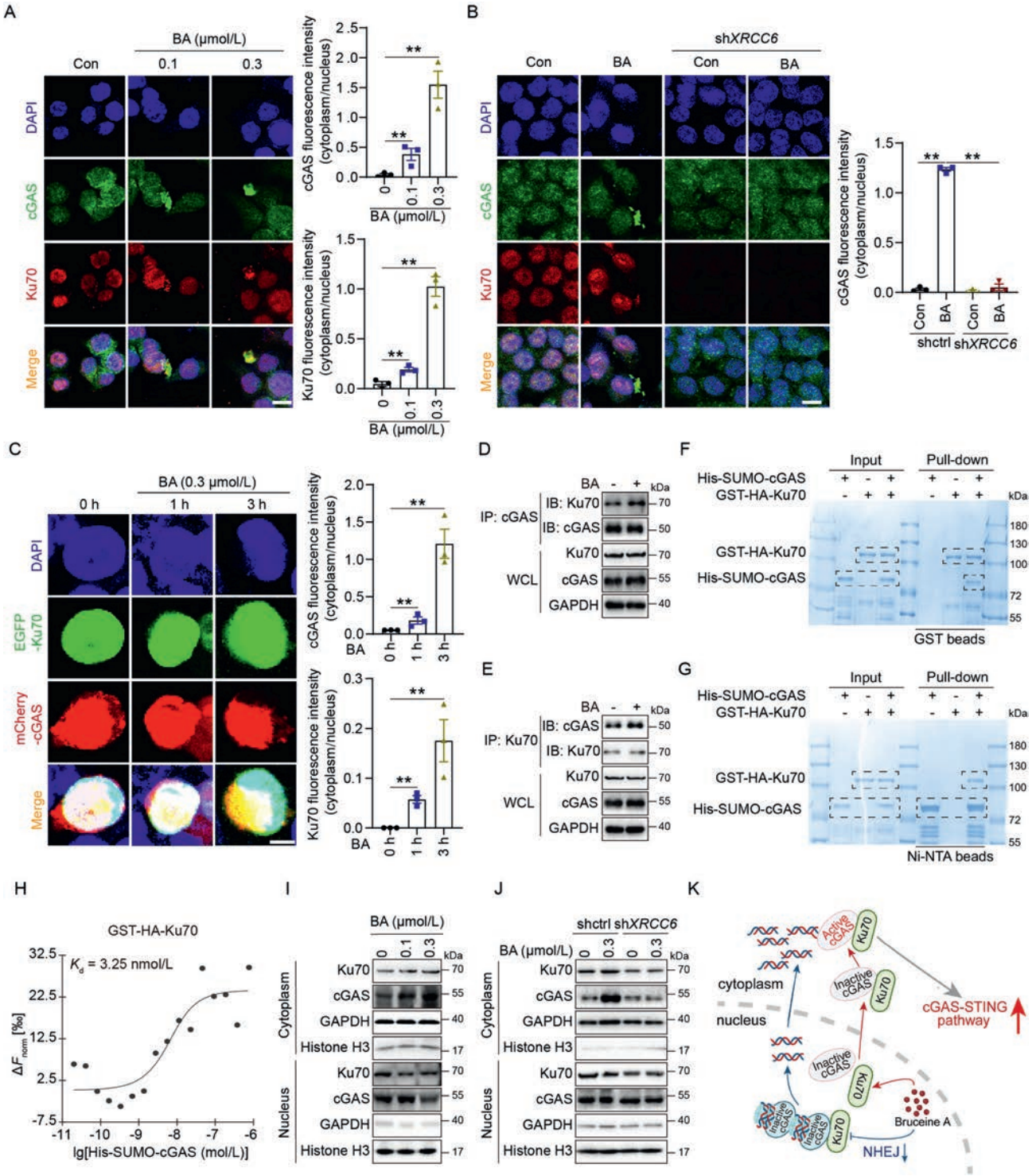

Figure 4 Bruceine A promoted cytoplasmic translocation of cGAS *via* Ku70 (A) Cellular immunofluorescence analysis for colocalization between cGAS and Ku70 in HCT-116 cells treated with Bruceine A (0.1 and 0.3 μmol/L) for 12 h. Quantitative analysis of Ku70 and cGAS is shown beside. Scale bar: 75 μm (B) Cellular immunofluorescence analysis for colocalization between cGAS and Ku70 in shctrl and sh*XRCC6* HCT-116 cells treated with Bruceine A (0.3 μmol/L). Quantitative analysis of cGAS is shown beside. Scale bar: 75 μm (C) HEK293T cells overexpressing the EGFP-Ku70 and mCherry-cGAS were treated with Bruceine A (0.3 μmol/L) for 1.5 and 3 h. Quantitative analysis of Ku70 and cGAS is shown beside. Scale bar: 10 μm (D, E) HCT-116 cells were exposed to Bruceine A (0.3 μmol/L) for 12 h, and the interaction between Ku70 and cGAS was performed using immunoprecipitation (F, G) Pull-down analysis for interaction between hKu70 and hcGAS (H) The hcGAS bound to hKu70 was detected using the MST assay (I) HCT-116 cells were exposed to Bruceine A (0.1 and 0.3 μmol/L) for 6 h, and Western blotting analysis for Ku70 and cGAS expression levels in the nucleus and cytoplasm (J) The shctrl or sh*XRCC6* HCT-116 cells were incubated with Bruceine A (0.3 μmol/L) for 6 h (K) Mechanism diagram for dsDNA release and transition from inactive cGAS to active cGAS by Ku70

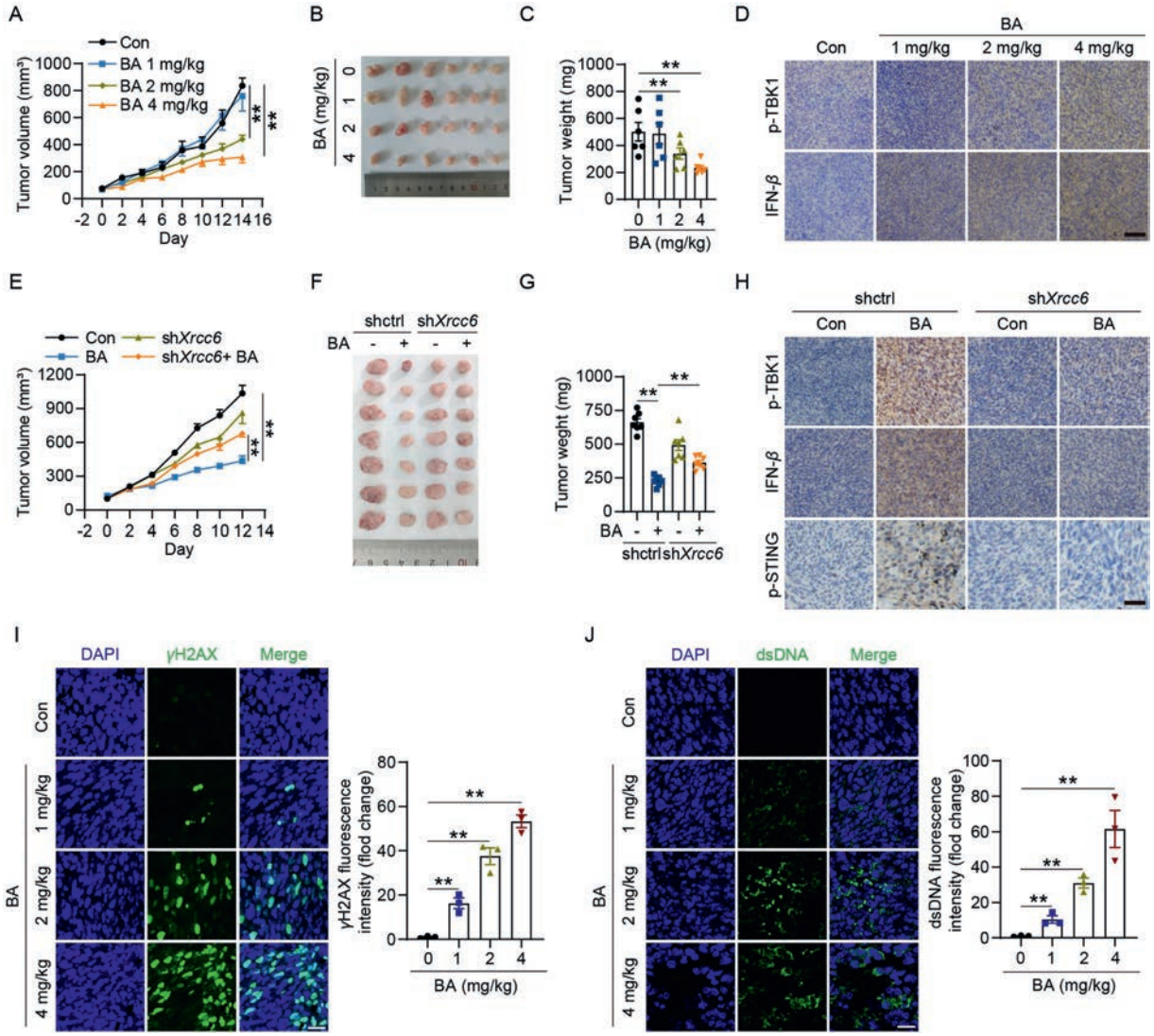

Figure 5 Bruceine A inhibits tumor growth *in vivo* through Ku70-dependent mechanisms (A−C) MC-38 cells (1×10^6 per mouse) were implanted into C57BL/6J mice and treated with Bruceine A (1, 2, and 4 mg/kg, i.p., once a day) from Day 0 to Day 14. The tumor volume and weight were recorded ($n = 6$ per group) (D) Immunohistochemical analysis for IFN-β and p-TBK1. Scale bars: 50 μm (E−G) C57BL/6 J mice bearing shctrl and sh*Xrcc6* MC-38 colon carcinoma cells (1×10^6 per mouse) were treated with Bruceine A (4 mg/kg, i.p., once a day) from Day 0 to Day 12. The tumor volume and weight were recorded ($n = 7$ per group) (H) Immunohistochemical analysis of IFN-β, p-TBK1, and p-STING. Scale bars: 50 μm (I, J) Tissue immunofluorescence for γH2AX and dsDNA. Quantitative analysis of γH2AX and dsDNA is shown beside. Scale bar: 75 μm. The *P* values are indicated, $^{**}P < 0.01$. Data are presented as mean ± SEM. Statistical analysis was performed using one-way ANOVA with Dunn's multiple-comparison test.

especially among individuals under 50 years of age. Despite advances in treatment options, such as chemotherapy, targeted therapy, and immunotherapy, the overall prognosis for patients with advanced or metastatic CRC remains poor due to therapeutic resistance and tumor progression[53,54]. Thus, there is an urgent need for novel treatment strategies that can enhance anti-tumor immunity and overcome resistance to current therapies. In this study, we identified Bruceine A, a small molecular compound derived from *Brucea javanica*, as a potent activator of the cGAS−STING pathway, which plays a crucial role in immune surveillance and anti-tumor immunity. Our findings not only elucidate the mechanism by which Bruceine A activates

protein under Bruceine A stimulation to trigger cGAS−STING and interferon signals in the tumor microenvironment. The *P* values are indicated, $^{**}P < 0.01$. Data are presented as mean ± SEM. Statistical analysis was performed using one-way ANOVA with Dunn's multiple-comparison test.

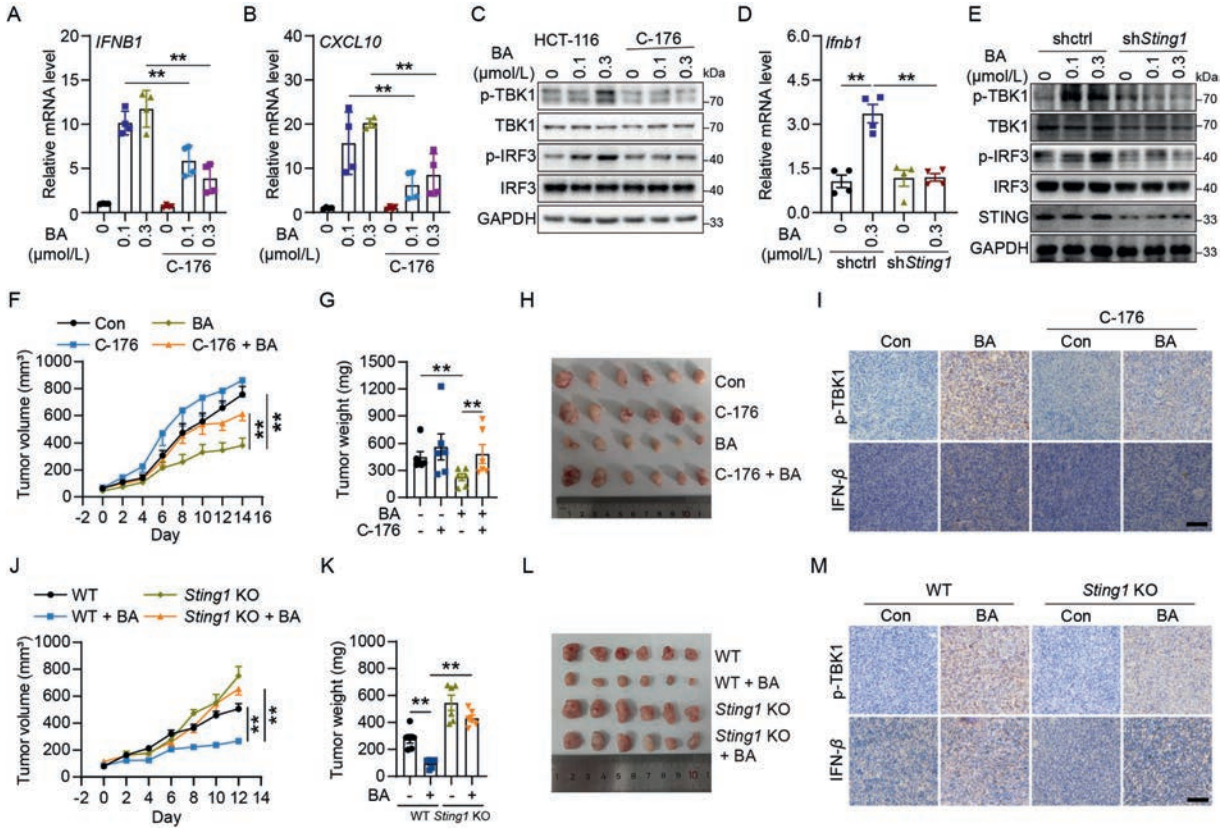

Figure 6 Bruceine A suppresses tumor growth through STING activation (A, B) HCT-116 cells were treated with Bruceine A (0.1 and 0.3 μmol/L) and C-176 (1 μmol/L) for 12 h, and the mRNA levels of *IFNB1* and *CXCL10* were detected by RT-qPCR (C) Western blotting analysis of p-TBK1, TBK1, p-IRF3, and IRF3 in HCT-116 cells treated with Bruceine A (0.1 and 0.3 μmol/L) and C-176 (1 μmol/L) for 6 h (D) MC-38 cells were transfected with sh*Sting1* lentivirus, followed by Bruceine A (0.3 μmol/L) stimulation for 12 h, and the *Ifnb1* mRNA expression level was detected using RT-qPCR (E) Western blotting analysis of p-TBK1, TBK1, p-IRF3, IRF3, and Ku70 in shctrl and sh*Sting1* MC-38 cells treated with Bruceine A (0.1 and 0.3 μmol/L) for 6 h (F−H) C57BL/6 J mice bearing MC-38 colon carcinoma cells (1×10^6 per mouse) were treated with Bruceine A (4 mg/kg, i.p., once a day) and C-176 (14.4 mg/kg, i.p., once a day) from Day 0 to Day 14. The tumor volume and weight were recorded ($n = 6$ per group) (I, M) Immunohistochemical analysis of IFN-β and p-TBK1. Scale bars: 50 μm (J−L) C57BL/6 J wild type and *Sting1* KO mice bearing MC-38 colon carcinoma cells (1×10^6 per mouse) were treated with Bruceine A (4 mg/kg i.p., once a day) from Day 0 to Day 12. The tumor volume and weight were recorded ($n = 6$ per group). The P values are indicated, $^{**}P < 0.01$. Data are presented as mean ± SEM. Statistical analysis was performed using one-way ANOVA with Dunn's multiple-comparison test.

cGAS−STING signaling but also reveal how Ku70 mediates this process, offering new insights into potential therapeutic strategies for CRC.

The cGAS−STING pathway is a critical component of the innate immune response, particularly in the detection of cytosolic DNA. Upon sensing double-stranded DNA (dsDNA), cGAS catalyzes the production of cGAMP, which activates STING and subsequently induces type I interferon signaling. This pathway has been shown to enhance anti-tumor immunity by promoting the activation of immune cells, including $CD8^+$ T cells. However, despite its potential as a therapeutic target, the activation of this pathway in tumor cells remains challenging due to the need for proper cellular localization and the release of dsDNA. Our study demonstrates that Bruceine A facilitates cGAS−STING activation through a novel mechanism involving cGAS translocation from the nucleus to the cytoplasm. This process is mediated by Ku70, a DNA damage repair protein that has recently been shown to play roles beyond its nuclear function. Targeting Ku70 using Bruceine A promotes cGAS relocation to the cytoplasm, where it can effectively sense dsDNA, leading to STING activation and the subsequent anti-tumor immune response.

Importantly, our findings also highlight the dual roles of Ku70 in both DNA damage repair and immune activation. Under normal conditions, Ku70 is primarily involved in the repair of DNA double-strand breaks through the non-homologous end joining (NHEJ) pathway[23]. However, we show that Bruceine A inhibits NHEJ and induces the release of dsDNA, thereby enhancing cGAS−STING signaling. This is further supported by the observation that genetic ablation of Ku70 results in increased γH2AX expression and elevated levels of cytoplasmic dsDNA, suggesting that Ku70's role in DNA repair is essential for maintaining genomic stability. Moreover, Bruceine A inhibits DNA repair and promotes dsDNA release to trigger the activation of cGAS−STING signal, providing a mechanism by which Bruceine A can enhance the immune response against tumors.

Our *in vivo* studies further confirmed the anti-tumor efficacy of Bruceine A, showing that it effectively inhibits tumor growth in murine models through Ku70-dependent activation of the

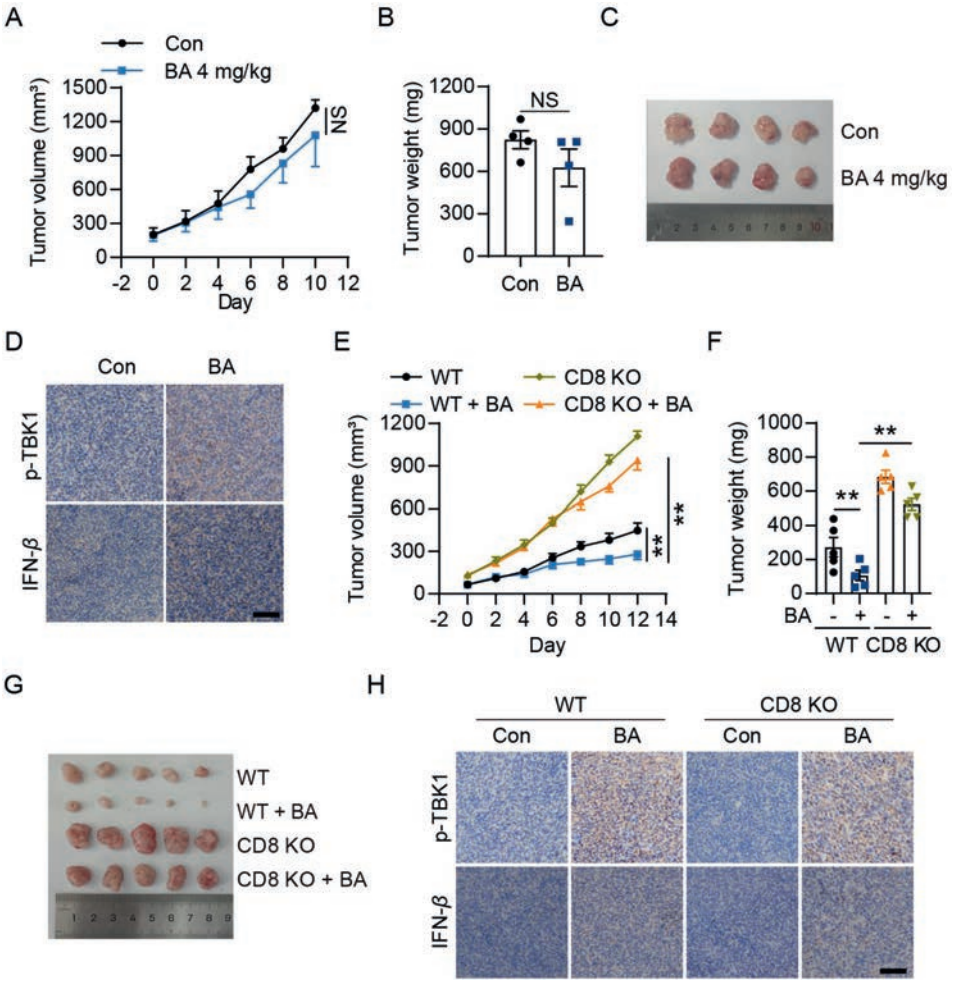

Figure 7 Inhibition of tumor growth induced by Bruceine A depends on the host's immune response (A−C) BALB/c nude mice bearing MC-38 colon carcinoma cells (1×10^6 per mouse) were treated with Bruceine A (4 mg/kg, i.p., once a day). The tumor volume and weight were recorded ($n = 4$ per group) (D) Immunohistochemical analysis of IFN-β and p-TBK1. Scale bars: 50 μm (E−G) C57BL/6 J wild type and CD8 KO mice bearing MC-38 colon carcinoma cells (1×10^6 per mouse) were treated with Bruceine A (4 mg/kg, i.p., once a day). The tumor volume and weight were recorded ($n = 5$ per group) (H) Immunohistochemical analysis of IFN-β and p-TBK1. Scale bars: 50 μm. The *P* values are indicated, $^{**}P < 0.01$; NS, not significant. Data are presented as mean ± SEM. Statistical analysis was performed using one-way ANOVA with Dunn's multiple-comparison test.

cGAS−STING pathway. Significantly, silencing Ku70 in tumor cells attenuated the anti-tumor effects of Bruceine A, underscoring the central role of Ku70 in mediating the compound's therapeutic effects. Additionally, we demonstrated that Bruceine A-induced anti-tumor immunity requires STING activation, as inhibition of STING or genetic ablation of STING abolished the tumor growth suppression induced by Bruceine A. These results indicate that Bruceine A not only activates cGAS−STING signaling in tumor cells but also induces a robust immune response through the production of type I interferons and enhanced $CD8^+$ T cell infiltration.

In conclusion, Bruceine A has the potential to sensitize conventional therapies of CRC, including chemotherapy, radiotherapy, and immunotherapy. We observed that the combination of Bruceine A with oxaliplatin, irradiation, and anti-PD-1 antibody enhanced tumor growth suppression and increased immune cell activation, particularly $CD8^+$ T cells. These findings suggest that Bruceine A can be effectively combined with standard CRC treatments to improve therapeutic outcomes, providing a promising strategy for overcoming resistance to current therapies.

Limitations of the study: Our study focuses on revealing the mechanism of Bruceine A activation of the cGAS−STING pathway and its potential application in colorectal cancer therapy. However, several key aspects of the molecular mechanism underlying Ku70-mediated cGAS nuclear export and activation remain to be elucidated. While we have investigated the effects of Bruceine A on-tumor cells and macrophages within the tumor microenvironment, the impact on lymphocyte populations and their functions remains unexplored. Although Ku70 is known to participate in diverse biological processes, the structural basis underlying its functional versatility and its relationship to the observed effects remains to be determined. Additionally, the long-term safety profile and potential off-target effects of Bruceine A warrant further investigation in pre-clinical models.

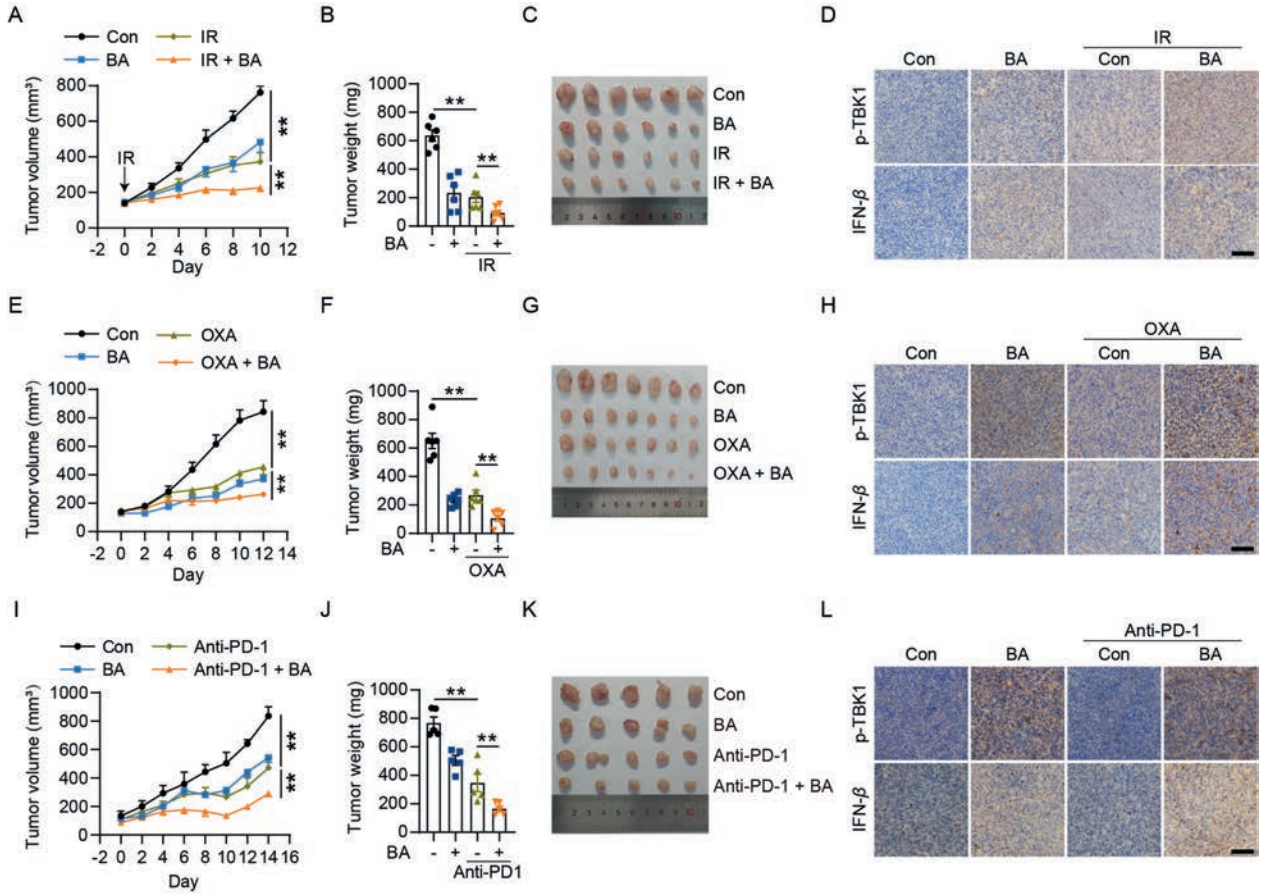

Figure 8 Bruceine A sensitizes radiotherapy, chemotherapy, and immunotherapy (A−C) C57BL/6 J mice bearing MC-38 colon carcinoma cells (1×10^6 per mouse) were treated with Bruceine A (4 mg/kg, i.p., once a day) from Day 0 to Day 10 and irradiation (IR, 3 Gy, once) on Day 0. The tumor volume and weight were recorded ($n = 6$ per group) (D) Immunohistochemical analysis of IFN-β and p-TBK1. Scale bars: 50 μm (E−G) C57BL/6 J mice bearing MC-38 colon carcinoma cells (1×10^6 per mouse) were treated with Bruceine A (4 mg/kg, i.p., once a day) and oxaliplatin (OXA, 2 mg/kg, i.p., twice a week) from Day 0 to Day 12. The tumor volume and weight were recorded ($n = 7$ per group) (H) Immunohistochemical analysis of IFN-β and p-TBK1. Scale bars: 50 μm (I−K) C57BL/6 mice bearing MC-38 colon carcinoma cells (1×10^6 per mouse) were treated with Bruceine A (4 mg/kg, i.p., once a day) and anti-PD-1 antibody (2 mg/kg, i.p., thrice a week) from Day 0 to Day 14. The tumor volume and weight were recorded ($n = 5$ per group) (L) Immunohistochemical analysis of IFN-β and p-TBK1. Scale bars: 50 μm. The P values are indicated, $^{**}P < 0.01$. Data are presented as mean ± SEM. Statistical analysis was performed using one-way ANOVA with Dunn's multiple-comparison test.

5. Conclusions

Our study reveals a novel mechanism through which Bruceine A enhances anti-tumor immunity in CRC by activating the cGAS−STING pathway *via* Ku70-mediated cGAS translocation from the nucleus to the cytoplasm. This mechanism not only enhances the immune response but also sensitizes tumors to chemotherapy, radiotherapy, and immunotherapy. Given its potential to synergize with existing treatment modalities, Bruceine A offers a promising therapeutic approach for CRC and warrants further clinical investigation to determine its efficacy in patients with advanced disease.

Acknowledgments

This work was supported by the National Natural Science Foundation of China (82473988, 82273933, 32201024, and 82202956, China), Key Project of Science and Technology in Jiangsu Province (BG2024007, China), and Fundamental Research Funds for the Central Universities (020814380199, 020814380201, China).

Author contributions

Kai Huang: writing-original draft, visualization, methodology, formal analysis, investigation. Zhaohui Tang: writing-original draft, visualization, methodology, data curation. Qin Gong: software, validation, formal analysis. Jianing Peng: methodology. Yicheng Rong: data curation, formal analysis. Tiancong Wu: resources. Weichen Song: methodology, investigation. Siyu Mao: methodology. Yugui Xia: methodology. Wenjie Guo: writing a review & editing, supervision, resources, project administration, data curation, conceptualization. Wen Liu: writing a review & editing, resources, project administration, funding acquisition, conceptualization.

Conflicts of interest

The authors declare no competing interests.

Appendix A. Supporting information

Supporting information to this article can be found online at https://doi.org/10.1016/j.apsb.2026.06.010.

References

1. Joshi BP, Dai Z, Gao Z, Lee JH, Ghimire N, Chen J, et al. Detection of sessile serrated adenomas in the proximal colon using wide-field fluorescence endoscopy. *Gastroenterology* 2017;**152**:1002−13.e9.
2. Yue Y, Hur J, Cao Y, Tabung FK, Wang M, Wu K, et al. Prospective evaluation of dietary and lifestyle pattern indices with risk of colorectal cancer in a cohort of younger women. *Ann Oncol* 2021;**32**:778−86.
3. Zhao G, Yuan H, Li Q, Zhang J, Guo Y, Feng T, et al. DDX39B drives colorectal cancer progression by promoting the stability and nuclear translocation of PKM2. *Signal Transduct Targeted Ther* 2022;**7**:275.
4. Liu S, Lin H, Wang D, Li Q, Luo H, Li G, et al. PCDH17 increases the sensitivity of colorectal cancer to 5-fluorouracil treatment by inducing apoptosis and autophagic cell death. *Signal Transduct Targeted Ther* 2019;**4**:53.
5. Dong G, He X, Chen Y, Cao H, Wang J, Liu X, et al. Genetic variations in genes of metabolic enzymes predict postoperational prognosis of patients with colorectal cancer. *Mol Cancer* 2015;**14**:171.
6. Sung H, Ferlay J, Siegel RL, Laversanne M, Soerjomataram I, Jemal A, et al. Global cancer statistics 2020: GLOBOCAN estimates of incidence and mortality worldwide for 36 cancers in 185 countries. *CA Cancer J Clin* 2021;**71**:209−49.
7. Wheeler DA, Takebe N, Hinoue T, Hoadley KA, Cardenas MF, Hamilton AM, et al. Molecular features of cancers exhibiting exceptional responses to treatment. *Cancer Cell* 2021;**39**:38−53.e7.
8. Li X, Wang J, Lin W, Yuan Q, Lu Y, Wang H, et al. circEXOC6B interacting with RRAGB, an mTORC1 activator, inhibits the progression of colorectal cancer by antagonizing the HIF1A−RRAGB−mTORC1 positive feedback loop. *Mol Cancer* 2022;**21**:135.
9. Li Y, Yang C, Liu Z, Du S, Can S, Zhang H, et al. Integrative analysis of CRISPR screening data uncovers new opportunities for optimizing cancer immunotherapy. *Mol Cancer* 2022;**21**:2.
10. Li Z, Zhang Q, Li Z, Ren L, Pan D, Gong Q, et al. Branched glycopolymer prodrug-derived nanoassembly combined with a STING agonist activates an immuno-supportive status to boost anti-PD-L1 antibody therapy. *Acta Pharm Sin B* 2024;**14**:2194−209.
11. Zhang Q, Tang Z, An R, Ye L, Zhong B. USP29 maintains the stability of cGAS and promotes cellular antiviral responses and autoimmunity. *Cell Res* 2020;**30**:914−27.
12. Lv M, Chen M, Zhang R, Zhang W, Wang C, Zhang Y, et al. Manganese is critical for antitumor immune responses *via* cGAS−STING and improves the efficacy of clinical immunotherapy. *Cell Res* 2020;**30**:966−79.
13. Xu H, Qin X, Guo Y, Zhao S, Feng X, Zhang R, et al. Radiation-based immunogenic vaccine combined with a macrophage "checkpoint inhibitor" for boosting innate and adaptive immunity against metastatic colon cancers. *Acta Pharm Sin B* 2024;**14**:2247−62.
14. Deng L, Liang H, Xu M, Yang X, Burnette B, Arina A, et al. STING-dependent cytosolic DNA sensing promotes radiation-induced type I interferon-dependent antitumor immunity in immunogenic tumors. *Immunity* 2014;**41**:843−52.
15. Gao D, Wu J, Wu YT, Du F, Aroh C, Yan N, et al. Cyclic GMP−AMP synthase is an innate immune sensor of HIV and other retroviruses. *Science* 2013;**341**:903−6.
16. Zhang C, Shang G, Gui X, Zhang X, Bai XC, Chen ZJ. Structural basis of STING binding with and phosphorylation by TBK1. *Nature* 2019;**567**:394−8.
17. Marcus A, Mao AJ, Lensink-Vasan M, Wang L, Vance RE, Raulet DH. Tumor-derived cGAMP triggers a STING-mediated interferon response in non-tumor cells to activate the NK cell response. *Immunity* 2018;**49**:754−63.e4.
18. Zhao B, Xu P, Rowlett CM, Jing T, Shinde O, Lei Y, et al. The molecular basis of tight nuclear tethering and inactivation of cGAS. *Nature* 2020;**587**:673−7.
19. Boyer JA, Spangler CJ, Strauss JD, Cesmat AP, Liu P, McGinty RK, et al. Structural basis of nucleosome-dependent cGAS inhibition. *Science* 2020;**370**:450−4.
20. Cao D, Han X, Fan X, Xu RM, Zhang X. Structural basis for nucleosome-mediated inhibition of cGAS activity. *Cell Res* 2020;**30**:1088−97.
21. Mackenzie KJ, Carroll P, Martin CA, Murina O, Fluteau A, Simpson DJ, et al. cGAS surveillance of micronuclei links genome instability to innate immunity. *Nature* 2017;**548**:461−5.
22. Zhang JN, Dong MM, Cao W, Chen HG, Gu HY, Feng YL, et al. Disruption of DNA−PKcs-mediated cGAS retention on damaged chromatin potentiates DNA damage-inducing agent-induced anti-multiple myeloma activity. *Br J Cancer* 2024;**131**:430−43.
23. Tao X, Song J, Song Y, Zhang Y, Yang J, Zhang P, et al. Ku proteins promote DNA binding and condensation of cyclic GMP−AMP synthase. *Cell Rep* 2022;**40**:111310.
24. Wilson JE, Petrucelli AS, Chen L, Koblansky AA, Truax AD, Oyama Y, et al. Inflammasome-independent role of AIM2 in suppressing colon tumorigenesis *via* DNA−PK and Akt. *Nat Med* 2015;**21**:906−13.
25. Shao L, Goronzy JJ, Weyand CM. DNA-dependent protein kinase catalytic subunit mediates T-cell loss in rheumatoid arthritis. *EMBO Mol Med* 2010;**2**:415−27.
26. Wang J, Kang L, Song D, Liu L, Yang S, Ma L, et al. Ku70 senses HTLV-1 DNA and modulates HTLV-1 replication. *J Immunol* 2017;**199**:2475−82.
27. Taffoni C, Marines J, Chamma H, Guha S, Saccas M, Bouzid A, et al. DNA damage repair kinase DNA−PK and cGAS synergize to induce cancer-related inflammation in glioblastoma. *EMBO J* 2023;**42**:e111961.
28. Zhang X, Brann TW, Zhou M, Yang J, Oguariri RM, Lidie KB, et al. Cutting edge: Ku70 is a novel cytosolic DNA sensor that induces type III rather than type I IFN. *J Immunol* 2011;**186**:4541−5.
29. Sui H, Zhou M, Imamichi H, Jiao X, Sherman BT, Lane HC, et al. STING is an essential mediator of the Ku70-mediated production of IFN-λ1 in response to exogenous DNA. *Sci Signal* 2017;**10**:5054.
30. Sui H, Chen Q, Imamichi T. Cytoplasmic-translocated Ku70 senses intracellular DNA and mediates interferon-lambda 1 induction. *Immunology* 2021;**163**:323−37.
31. Martinez JJ, Seveau S, Veiga E, Matsuyama S, Cossart P. Ku70, a component of DNA-dependent protein kinase, is a mammalian receptor for *Rickettsia conorii*. *Cell* 2005;**123**:1013−23.
32. Wang Y, Fu Z, Li X, Liang Y, Pei S, Hao S, et al. Cytoplasmic DNA sensing by KU complex in aged $CD4^+$ T cell potentiates T cell activation and aging-related autoimmune inflammation. *Immunity* 2021;**54**:632−47.e9.
33. Hu J, Liu W, Zou Y, Jiao C, Zhu J, Xu Q, et al. Allosterically activating SHP2 by oleanolic acid inhibits STAT3−Th17 axis for ameliorating colitis. *Acta Pharm Sin B* 2024;**14**:2598−612.
34. Yang J, Jiao C, Liu N, Liu W, Wang Y, Pan Y, et al. *Polydatin-mediated inhibition of HSP90α disrupts NLRP3 complexes and alleviates acute pancreatitis*vol. 7. Research (Wash D C); 2024. p. 551.
35. Wang Y, Wei B, Wang D, Wu J, Gao J, Zhong H, et al. DNA damage repair promotion in colonic epithelial cells by andrographolide downregulated cGAS−STING pathway activation and contributed to the relief of CPT-11-induced intestinal mucositis. *Acta Pharm Sin B* 2022;**12**:262−73.
36. Martinez Molina D, Jafari R, Ignatushchenko M, Seki T, Larsson EA, Dan C, et al. Monitoring drug target engagement in cells and tissues using the cellular thermal shift assay. *Science* 2013;**341**:84−7.
37. Zhou W, Whiteley AT, de Oliveira Mann CC, Morehouse BR, Nowak RP, Fischer ES, et al. Structure of the human cGAS−DNA

complex reveals enhanced control of immune surveillance. *Cell* 2018; **174**:300−11.e11.
38. Hanakahi LA. 2-Step purification of the Ku DNA repair protein expressed in *Escherichia coli*. *Protein Expr Purif* 2007;**52**:139−45.
39. Ghosh M, Saha S, Bettke J, Nagar R, Parrales A, Iwakuma T, et al. Mutant p53 suppresses innate immune signaling to promote tumorigenesis. *Cancer Cell* 2021;**39**:494−508.e5.
40. Spagnolo L, Rivera-Calzada A, Pearl LH, Llorca O. Three-dimensional structure of the human DNA-PKcs/Ku70/Ku80 complex assembled on DNA and its implications for DNA DSB repair. *Mol Cell* 2006;**22**:511−9.
41. Mao Z, Seluanov A, Jiang Y, Gorbunova V. TRF2 is required for repair of nontelomeric DNA double-strand breaks by homologous recombination. *Proc Natl Acad Sci U S A* 2007;**104**:13068−73.
42. Collis SJ, DeWeese TL, Jeggo PA, Parker AR. The life and death of DNA−PK. *Oncogene* 2005;**24**:949−61.
43. Lv G, Wang Q, Lin L, Ye Q, Li X, Zhou Q, et al. mTORC2-driven chromatin cGAS mediates chemoresistance through epigenetic reprogramming in colorectal cancer. *Nat Cell Biol* 2024;**26**:1585−96.
44. Michalski S, de Oliveira Mann CC, Stafford CA, Witte G, Bartho J, Lammens K, et al. Structural basis for sequestration and autoinhibition of cGAS by chromatin. *Nature* 2020;**587**:678−82.
45. Cho MG, Kumar RJ, Lin CC, Boyer JA, Shahir JA, Fagan-Solis K, et al. MRE11 liberates cGAS from nucleosome sequestration during tumorigenesis. *Nature* 2024;**625**:585−92.
46. Sun H, Huang Y, Mei S, Xu F, Liu X, Zhao F, et al. A nuclear export signal is required for cGAS to sense cytosolic DNA. *Cell Rep* 2021;**34**: 108586.
47. Haag SM, Gulen MF, Reymond L, Gibelin A, Abrami L, Decout A, et al. Targeting STING with covalent small-molecule inhibitors. *Nature* 2018;**559**:269−73.
48. Woo SR, Fuertes MB, Corrales L, Spranger S, Furdyna MJ, Leung MY, et al. STING-dependent cytosolic DNA sensing mediates innate immune recognition of immunogenic tumors. *Immunity* 2014; **41**:830−42.
49. Hou Y, Liang H, Rao E, Zheng W, Huang X, Deng L, et al. Non-canonical NF-κB antagonizes STING sensor-mediated DNA sensing in radiotherapy. *Immunity* 2018;**49**:490−503.e4.
50. Xu Y, Xiang Z, Alnaggar M, Kouakanou L, Li J, He J, et al. Allogeneic Vγ9Vδ2 T-cell immunotherapy exhibits promising clinical safety and prolongs the survival of patients with late-stage lung or liver cancer. *Cell Mol Immunol* 2021;**18**:427−39.
51. Prise KM, O'Sullivan JM. Radiation-induced bystander signalling in cancer therapy. *Nat Rev Cancer* 2009;**9**:351−60.
52. Gillison ML, Trotti AM, Harris J, Eisbruch A, Harari PM, Adelstein DJ, et al. Radiotherapy plus cetuximab or cisplatin in human papillomavirus-positive oropharyngeal cancer (NRG oncology RTOG 1016): a randomised, multicentre, non-inferiority trial. *Lancet* 2019; **393**:40−50.
53. Li F, Fang Z, Zhang J, Li C, Liu H, Xia J, et al. Identification of TRA2B-DNAH5 fusion as a novel oncogenic driver in human lung squamous cell carcinoma. *Cell Res* 2016;**26**:1149−64.
54. Pérez-Guijarro E, Yang HH, Araya RE, El Meskini R, Michael HT, Vodnala SK, et al. Multimodel preclinical platform predicts clinical response of melanoma to immunotherapy. *Nat Med* 2020;**26**:781−91.